Ellipse Inversion Model for Estimating the Orientation and Radius of Pipes From GPR Image

Xiren Zhou ⬛, Qiuju Chen, Shengfei Lyu, and Huanhuan Chen ⬛, *Senior Member, IEEE*

Abstract—Ground penetrating radar (GPR) has been widely used as a nondestructive tool to image the subsurface. When the GPR's detecting direction is perpendicular to the orientation of a buried pipeline, a hyperbolic feature would be formed on the GPR B-scan image, which could then be identified and fitted to estimate the target pipeline and the permittivity of the area. However, in real-world applications, the orientation of pipelines on the existing pipeline map could be inaccurate, and it is hard to ensure that the moving direction of GPR is actually perpendicular to the underground pipeline. In this article, a novel model is proposed to estimate the orientation and radius of the pipeline from the GPR B-scan image, provided the permittivity of the underground medium. The model consists of the following two parts: GPR B-scan image processing and ellipse iterative inversion algorithm (EIIA). First, the GPR B-scan image is processed with the downward-opening point set extracted. The obtained point set is then iteratively inverted to the elliptical cross-section of the buried pipeline, which is caused by the angle between the GPR's detecting direction and the pipeline's orientation. By minimizing the sum of the algebraic distances from the extracted point set to the inverted ellipse, the most likely pipeline's orientation and radius are determined. Experiments on real-world datasets are conducted and analyzed, of which the results demonstrate the effectiveness of the proposed model.

Index Terms—Buried pipeline detection, data processing, ground penetrating radar (GPR).

I. INTRODUCTION

UNDERGROUND pipelines are indispensable for the normal operation of urban cities, and part of pipelines are nearing their practical life and need to be replaced or repaired [1]. To locate the buried utilities and revise the existing pipeline map, ground penetrating radar (GPR) has been widely used due to its fast speed and minimal ground intrusion [2]. Existing studies mainly abstract the issue of estimating pipelines by GPR as a mathematical problem of hyperbolic extraction and fitting [3]. Considerable efforts have been devoted to this area, and many strategies have been employed to address this issue, including the Hough transform [4], [5], the machine learning methods [6], [7], [8], and some combinations of several kinds of methods [9], [10], [11]. However, using hyperbolic fitting methods to obtain pipeline information from GPR images needs to satisfy some non-negligible constraints: 1) The pipeline needs to be horizontally buried within the effective depth range of the utilized GPR with different permittivity from the surrounding medium [12], and the dimension of the pipeline should be within the resolvable range of the used antenna. 2) The detecting direction of GPR should be perpendicular to the pipeline, thus, there would be a standard hyperbolic curve on the GPR B-scan image [13]. In real-world applications, the direction of the buried pipeline could be rarely precisely acknowledged. The nonperpendicular detection angle will result in nonstandard hyperbolic curves on the GPR image, which will lead to unreliable hyperbolic fitting results. Moreover, GPR images could be noisy due to the system noise, the heterogeneity of the medium, and mutual wave interactions. Obtaining the three parameters of radius, depth, and dielectric constant at the same time in such a noisy environment could lead to nonunique optimization results, which also reduces the reliability of hyperbolic-fitting.

When estimating underground pipelines using GPR, the subsurface permittivity is an important parameter, and it is related to the speed at which electromagnetic waves propagate underground. The most direct method to estimate the subsurface permittivity is by comparing the resolution of the GPR image with the actual target depth [12]. This kind of methods requires accurate measurement of the subsurface target's depth by moderate excavation, or through manhole covers and other means that can directly observe the subsurface. Several algorithms have been developed to determine the subsurface permittivity from GPR data [14], [15]. Basically, two reflections could be used to calculate the permittivity of the subsurface [16]. Besides the abovementioned methods, as aforementioned, the permittivity of the underground medium could also be estimated by fitting the hyperbolic feature generated by the pipeline on the GPR B-scan image. Some GPR data processing tools, such as GPR SLICE, GSSI RADAN, or MATGPR [17], provide means to manually fit the hyperbolic curves generated by the underground pipeline. Although limitations exist when conducting hyperbolic fitting, it is feasible to form one or several standard hyperbolic curves with less noise, regular shape, and edges in the obtained GPR

Xiren Zhou and Huanhuan Chen are with the School of Computer Science and Technology, University of Science and Technology of China, Hefei 230027, China (e-mail: zhou0612@mail.ustc.edu.cn; hchen@ustc.edu.cn).

Qiuju Chen is with the School of Information Science and Technology, University of Science and Technology of China, Hefei 230027, China (e-mail: qqchern@ustc.edu.cn).

Shengfei Lyu is with the Nanyang Technological University, Singapore 639798 (e-mail: shengfei.lyu@ntu.edu.sg).

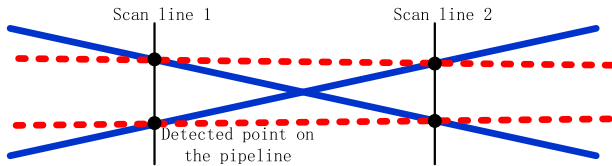Digital Object Identifier 10.1109/JSTARS.2022.3205889

Fig. 1. Example of misconnecting detected points on the pipeline, resulting in a wrong pipeline map. The black lines represent two parallel GPR scan lines, and the black dots represent the detected points on the pipelines. The red dotted lines are used to connect these detected points regardless of the pipelines' orientation, while the actual situation is shown by the blue lines. Therefore, adopting the red dotted lines results in a wrong pipeline map.

image, and fit these curves to estimate the permittivity of the detected area.

Once the permittivity of the detected area is obtained through the abovementioned methods, the ordinate of the GPR B-scan image could be converted from time to depth [18]. When detecting other pipelines in this area, their depth could be directly inferred from the GPR B-scan image [19]. The follow-up work is to further estimate the orientation and radius of other pipelines in the detected area from GPR data. In [20], the orientation of the underground pipeline is roughly inferred by the statutory records of buried facilities, and parallel GPR detections are then conducted to derive the specific orientation of each pipeline by connecting the tops of identified hyperbolic features on the obtained B-scan images. In [21], [22], and [23], the orientation and location of a pipeline are obtained by fitting several detected points on the pipeline. The abovementioned methods mainly determine the orientation of a pipeline by connecting or fitting the results of multiple detections. As Fig. 1 shows, when mapping multiple pipelines, if the directions of the pipelines are not estimated and considered, the results of connecting or fitting the detected points could be inconsistent with the actual situation. If the hyperbolic-fitting method is used to confirm the radius and orientation of a pipeline, two measurements should be required to determine the pipeline's orientation, and one more measurement is needed to obtain the exact radius. In real-world applications, multiple detections might increase the data acquisition time. Moreover, when the pipeline's orientation is not perpendicular to the GPR's detecting direction, it could be inaccurate to measure the radius of pipelines by fitting hyperbolic features on the B-scan image, since the cross-section of the pipeline on the GPR's detecting direction is an ellipse instead of a circle.

In addition to the abovementioned methods, there are some published methods [24], [25], [26], [27] that estimate the orientation of a subsurface linear target through polarimetric GPR data. In [24], the linearity factor is used to classify rotationally symmetric and linear objects, which is estimated from the eigenvalues of the scattering matrix obtained from polarimetric GPR data. A linear target has a preferential scattering axis that coincides with its long axis [25]. The strike direction of a subsurface fracture could be estimated by minimizing the energy of the cross-polarized components, which is realized by zeroing the derivative of the energy in the cross-polarization channel [26]. In [27], a hybrid dual-polarimetric GPR system,

which consists of a circularly polarized transmitting antenna and two linearly polarized receiving antennas, is employed to estimate buried linear objects. A full-polarimetric scattering matrix is extracted from the double-channel GPR signals reflected from a buried linear object, and then an improved Alford rotation method is utilized to estimate the orientation angle of the object from the extracted scattering matrix. The aforementioned methods identify the orientation of linear targets mainly from the scattering matrix extracted from the polarimetric GPR data. For given equipment and data, such as the GSSI's SIR-30 GPR utilized in this article and the obtained B-scan images, effective methods are still needed to measure the orientation or radius of the underground pipeline.

In this article, the ellipse inversion model is proposed to estimate the orientation and radius of the pipeline from the GPR B-scan image. Unlike hyperbolic fitting, the proposed model reduces the parameters to be solved. The detecting direction of the GPR is not required to be perpendicular to the pipeline's orientation, and only one detection is required to measure the orientation and radius of the pipeline. There are the following two prerequisites for conducting the proposed model: 1) The relative permittivity near the pipeline needs to be acknowledged. 2) Similar to the hyperbolic fitting task, the depth of the underground pipeline should be within the effective detecting depth of the utilized GPR, and the dimension of the pipeline should be within the resolvable range of the used GPR. The proposed model consists of the following two parts: GPR B-scan image processing and the ellipse iterative inversion algorithm (EIIA). The GPR B-scan image is first processed with the downward-opening point set extracted by extending part of our previous work [19]. As the angle between the GPR's detecting directions and the pipeline's orientation might not be perpendicular, the cross-section of the pipeline could be elliptical. In this case, the EIIA iteratively inverts the extracted downward-opening point set to the elliptical cross-section of the pipeline. By minimizing the sum of the algebraic distances from these points to the inverted ellipse, the most likely orientation and radius of the target pipeline are determined. The procedure of the proposed ellipse inversion model is presented in Fig. 2.

In the conducted experiments, the proposed model is combined with the GPR B-scan image interpreting method that has been detailed in our previous work [19]. Specifically, it is to determine the direction of a certain pipeline [28], and accurately measure the subsurface permittivity by extracting and fitting the generated hyperbola, and then the proposed ellipse inversion model is utilized to estimate other pipelines in the detection area. The experimental results validate the accuracy and efficiency of the proposed model.

The rest of this article is organized as follows. The GPR B-scan image processing is discussed in Section II. Section III provides the EIIA. Experiments are conducted and analyzed in Section IV. Finally, Section V concludes this article.

II. GPR B-SCAN IMAGE PROCESSING

In this section, the downward-opening signature on GPR B-scan images generated from the elliptical cross-section is
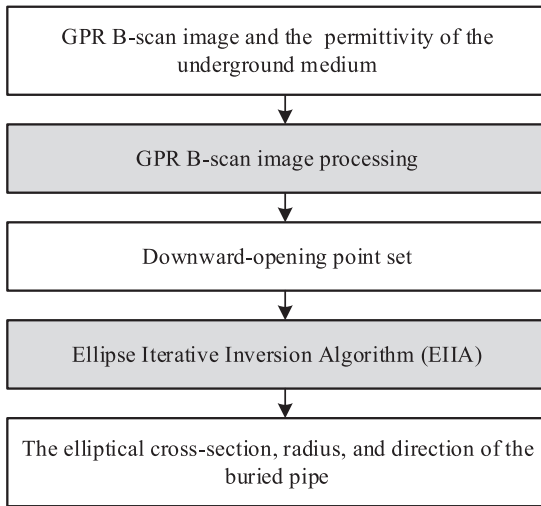
Fig. 2. Procedure of the proposed ellipse inversion model, which consists of the following two parts: GPR B-scan image processing and EIIA. Grey blocks refer to processing parts, which lead to various statuses of the data illustrated in white rectangular boxes.
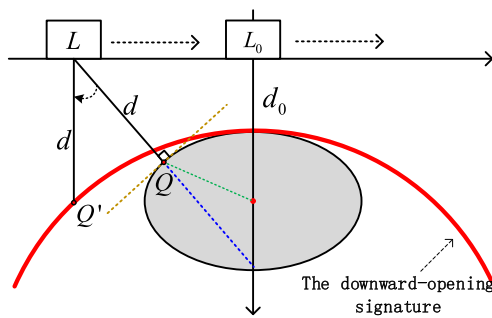

Fig. 3. Gray ellipse indicates the cross-section of the pipe. L is the location of the GPR, and L_0 means the location where the GPR is directly above the pipeline. Q is the closest point on the ellipse to the GPR position L, and the distance from L to the ellipse is $|LQ| = d$. The red line indicates the downward-opening signature generated by the pipeline on the GPR B-scan image. Q' is the point on the downward-opening signature directly below L generated by Q, which could be regarded as the result of the rotation of LQ around L to the vertical below of L, and the length d of LQ remains unchanged during the rotation process, that is, $|LQ| = |LQ'| = d$.

analyzed. Then, the method to extract the point set with downward-opening signature is introduced.

A. Downward-Opening Signatures Generated by the Elliptical Cross-Section

Fig. 3 illustrates the schematic diagram when the GPR's detecting direction is not perpendicular to the pipeline's orientation, where the cross-section of the pipeline is elliptical. It could be observed that when the GPR is at L, the extension line (blue dotted line) of LQ, which indicates the distance d between the GPR and the ellipse, does not pass through the center[1] of the ellipse, as the blue and the green dashed lines do not coincide in Fig. 3. Q' is the mapped point observed by Q on the GPR image

[1]The center of the ellipse is the midpoint between the two focal points of the ellipse.

(perpendicular below L). Therefore, the feature produced by the elliptical cross-section on the GPR B-scan image could not be described by the hyperbolic equation [12]. As GPR moves from L to L_0, the distance between it and the pipeline gradually decreases. The trajectory when the GPR moves gradually away from L_0 is symmetrical, thus, the feature produced by the elliptical cross-section on the GPR B-scan image could be represented by the red downward-opening curve in Fig. 3.

In Fig. 3, the point Q' on the downward-opening curve could be regarded as the result of the rotation of LQ around L to the vertical below of L, and the length d of LQ remains unchanged during the rotation process, that is, $|LQ| = |LQ'| = d$. In the method proposed later in this article, the points on the downward-opening curves are extracted and gradually inverted to the elliptical cross-section where these points were generated, and the direction and radius of the pipe are inferred based on the inverted cross-section.

B. Extract Point Set With Downward-Opening Signatures

To eliminate the noise and highlight the targets, some operations need to be conducted on the obtained GPR B-scan image, which consists of the following three tasks:
1) eliminating the undesired presence of the ground surface echo;
2) reducing noise;
3) compensating propagation losses.

First, the reflectance of the ground surface is eliminated in advance. This work is supported by the Matgpr [17], which is a freeware MATLAB package for the analysis of common-offset GPR data. Then, a filtering step based on the standard median filter is performed [29] to reduce the electromagnetic noise and interferences. Finally, concerning the compensation of the propagation losses caused by the medium attenuation and the signal energy radial dispersion, a nonlinear time-varying gain is applied to the received signal [30].

After the abovementioned operations, the process of extracting the downward-opening point set from GPR B-scan images consists of the following four steps: preprocessing method, the open-scan clustering algorithm (OSCA), the parabolic fitting-based judgment (PFJ) method, and point set extracting. In the preprocessing method, the GPR B-scan image is first thresholded into the binary image based on the gray value on the boundary, and then the opening and closing operations [31] are applied to smooth the contour of the objects, eliminate small protrusions and fill small gaps in the contour noisy points. After that, OSCA scans the binary image progressively from top to bottom, finds the openings, and conducts clustering. Point clusters with downwardly-opening signatures are identified and extracted during the process of OSCA. PFJ further validates whether the identified downwardly-opening point clusters are symmetrical with the apex. The abovementioned operations and three steps have been detailed in our previous work [19], and experiments on both metal and cement pipelines are conducted, thus, they are not expanded in this article.

After the abovementioned steps, as the top of the pipeline is closest to the surface and the generated feature on the image
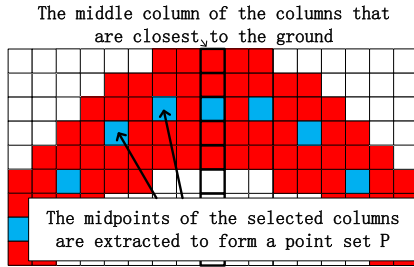
Fig. 4. Columns that are closest to the ground are identified, of which the middle one is selected as the central column. Then, we select several columns symmetrically at a certain interval on the left and right sides of the central column, and the midpoints of the selected columns are extracted to form the point set **P**.

Fig. 6. First coordinate conversion of P_i. Initially, the line at $P_i, P_{i,X}$ is perpendicular to the X-axis The gray ellipse represents the elliptical pipeline section fitted before coordinate conversion.

A. Ellipse Fitting Algorithm

The fitting of a general conic can be approached by minimizing the sum of squared algebraic distances $D(\mathbf{P})$ of the curve [32] to the point set $\mathbf{P} = \{(x_i, y_i)|1 \le i \le n\}$ as

$$\text{argmin } D(\mathbf{P}) = \sum_{i=1}^{n} F(\mathbf{A}, \mathbf{x_i})^2 \tag{2}$$

$$F(\mathbf{A}, \mathbf{x}) = \mathbf{A} \cdot \mathbf{x} = Ax^2 + Bxy + Cy^2 + Dx + Ey + F \tag{3}$$

where $\mathbf{A} = [A, B, C, D, E, F]^T$, $\mathbf{x} = [x^2, xy, y^2, x, y, 1]$, and $F(\mathbf{A}, \mathbf{x})$ is the "algebraic distance" of a point (x, y) to the conic $F(\mathbf{A}, \mathbf{x}) = 0$. An ellipse could be presented as

$$\frac{(x - x_0)^2}{a^2} + \frac{(y - y_0)^2}{b^2} = 1. \tag{4}$$

By transforming (4) into the form of (3), the following equation is obtained:

$$b^2 x^2 + a^2 y^2 - 2b^2 x_0 x - 2a^2 y_0 y$$
$$+ \left(a^2 y_0^2 + b^2 x_0^2 - a^2 b^2\right) = 0. \tag{5}$$

Comparing (5) and (3), it could be seen $B = 0$. To ensure the fitted conic to be elliptical, $4AC = 1$ is utilized as the constraint to limit the fitted curve to be an ellipse. Therefore, fitting the point set **P** to an ellipse could be formulated as

$$\text{argmin } D(\mathbf{P}) = \sum_{i=1}^{n} F(\mathbf{A}, \mathbf{x_i})^2$$
$$\text{s.t. } B = 0, \ 4AC = -1 \tag{6}$$

which is a convex optimization (CVX) problem and could be solved by the method proposed in [33].

B. Updating the Coordinates of Each Point in **P**

Given the point set $\mathbf{P} = \{P_i(x_i, y_i)| 0 \le i \le n\}$ as (1), the projection of each point $P_i = (x_i, y_i)$ on the X axis is $P_{i,X}$, which is the position of the GPR that collects the signal at P_i. As Fig. 6 shows, **P** is first fitted into an ellipse. Then, P_i rotates around the point $P_{i,X}$ to $P_{i,1}$ with the angle of θ_1, where $|P_{i,X}P_i| = |P_{i,X}P_{i,1}|$ and the distance between $P_{i,X}$ and the fitted ellipse is the shortest, that is, the straight line determined
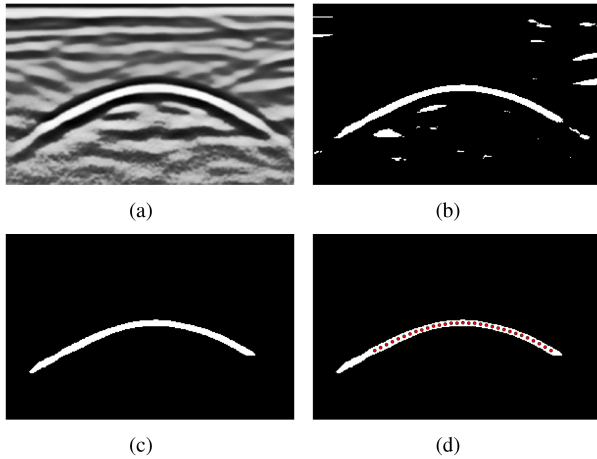

Fig. 5. Processing flow of extracting a downward-opening point set from a GPR B-scan image. (a) B-scan image obtained after the operations to eliminate the noise and highlight the targets. (b) Preprocessed binary image. (c) Obtained downward-opening point cluster after OSCA and PFJ. (d) Extracted point set from the downward-opening point cluster in (c).

is also the most obvious, the columns that are closest to the ground are further identified, of which the middle one is selected as the central column as shown in Fig. 4. Then, we select several columns symmetrically at a certain interval (3 cm in this article) on the left and right sides of the central column, and the midpoints of the selected columns are extracted to form a point set **P** as

$$\mathbf{P} = \{P_i(x_i, y_i) \mid 0 \le i \le n\} \tag{1}$$

which is further inverted to the elliptical cross-section of the buried pipeline. Fig. 5 illustrates the process of extracting a downward-opening point set from a GPR B-scan image.

III. ELLIPSE ITERATIVE INVERSION ALGORITHM

The EIIA aims to revert the downward-opening point set **P** to the elliptical cross-section of the pipe, which consists of the following two parts: the ellipse fitting, and updating **P** by converting the coordinates of each point. These two parts are detailed in this section followed by the settings of threshold in EIIA. The procedure of EIIA is finally presented.
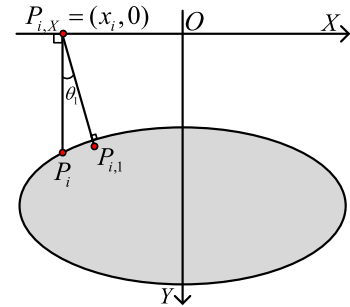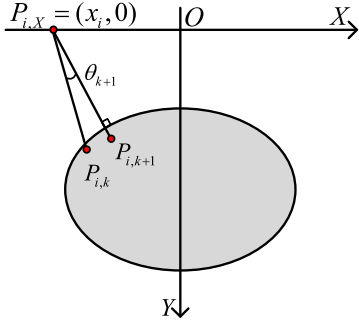
Fig. 7. $(k + 1)$th coordinate conversion of P_i. The gray ellipse represents the elliptical pipeline section fitted before coordinate conversion.
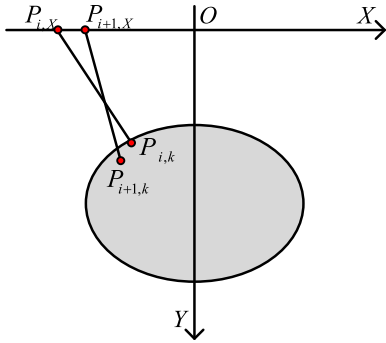

Fig. 8. Situation that $P_{i,k}$ is moved to the right side of $P_{i+1,k}$, although $P_{i,X}$ is at the left side of $P_{i+1,X}$. In this case, the rotated points in $\mathbf{P}$ would be out of order, which would lead to errors in the ellipse fitting.

by $P_{i,X}$ and $P_{i,1}$ is perpendicular to the tangent line at the closest intersection of the line and the fitted ellipse. The coordinates of $P_{i,1}$ could be obtained by

$$\begin{cases} x_{i,1} = x_i - y_i \sin \theta_1 \\ y_{i,1} = y_i \cos \theta_1 \end{cases} \tag{7}$$

where θ_1 could be obtained by calculating the shortest distance from a $P_{i,X}$ to the ellipse [34]. The rotation is applied on every point in $\mathbf{P}$, and the coordinates of these points are updated, by which $\mathbf{P}$ is updated to $\mathbf{P}_1 = \{P_{i,1}(x_{i,1}, y_{i,1}) \mid 0 \leq i \leq n\}$.

After kth iteration, as Fig. 7 shows, the coordinates of $P_{i,k+1}$ at the $k + 1$ iteration are updated as

$$\begin{cases} x_{i,k+1} = x_i - y_i \sin \left(\sum_{j=1}^{k+1} \theta_j \right) \\ y_{i,k+1} = y_i \cos \left(\sum_{j=1}^{k+1} \theta_j \right) \end{cases} \tag{8}$$

where θ_j is the jth rotating angle.

During the abovementioned operations, there might be a situation as Fig. 8 presented, where $P_{i,k}$ is moved to the right side of $P_{i+1,k}$, although $P_{i,X}$ is at the left side of $P_{i+1,X}$. In this case, the rotated points in $\mathbf{P}$ would be out of order, which is inconsistent with the actual pipeline and would lead to errors in the ellipse fitting. To avoid this situation, we set the order of each round of rotation in $\mathbf{P}$ to spread from the middle vertex to both the left and right sides. Meanwhile, once it is found that $P_{i,k}$ is rotated to the right side of $P_{i+1,k}$ as Fig. 8 shows, $P_{i,k}$ would be re-rotated to the left side of $P_{i+1,k}$, which is illustrated as $P'_{i,k}$
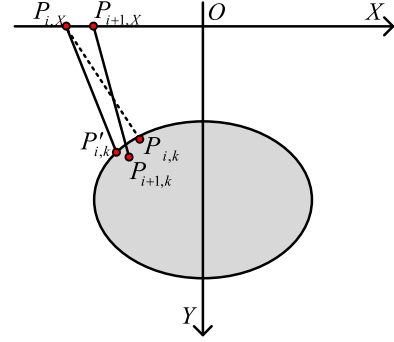
Fig. 9. Once it is found that $P_{i,k}$ is rotated to the right side of $P_{i+1,k}$ as the dashed line, $P_{i,k}$ would be rerotated to the left side of $P_{i+1,k}$ as $P'_{i,k}$, and the lateral distance between $P'_{i,k}$ and $P_{i+1,k}$ is set to be equal to the distance before $P_{i+1,k}$ is rotated.
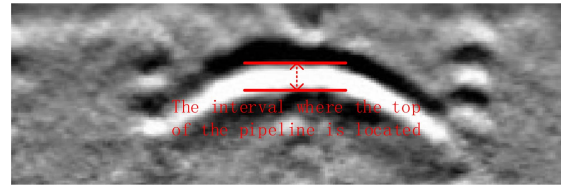

Fig. 10. Thickness of the wave (white bar) generated by the pipeline. The top of the pipeline should be in the center of the positive wave between the two red lines. The two-way travel time of the positive wave between the two red lines could be read out from the GPR image as Δt.

in Fig. 9, and the horizontal distance between $P'_{i,k}$ and $P_{i+1,k}$ is set to be equal to the distance before $P_{i+1,k}$ is rotated. With this constraint, the order of points in $\mathbf{P}$ would not change after each iteration, ensuring the normal operation of ellipse fitting.

The ellipse fitting and rotation are alternately and iteratively performed on $\mathbf{P}$. The condition for stopping the above iteration of fitting and rotation is that the iterative number reaches the preset threshold K, or the sum of algebraic distance $D(\mathbf{P})$ from each point in $\mathbf{P}$ to the fitted ellipse tends to be stable.

C. Threshold of the Algebraic Distance

The threshold D_t of the algebraic distance is not set to be a fixed value, but is mainly determined by the thickness (wavelength) of the wave generated by the pipeline on the GPR image. As Fig. 10 shows, the top of the pipeline should be in the center of the positive wave (white bar). The selected points to be fitted in the proposed model are also derived from the center of the positive wave. In our model, the subsurface permittivity is assumed to be acknowledged, thus, the speed of propagation of the EM wave could be obtained as v. The two-way travel time of the positive wave formed by the pipeline could be read out from the image as Δt. Therefore, the thickness d of the positive wave generated by the pipeline could be roughly estimated as

$$d = \frac{\Delta t}{2} \times v. \tag{9}$$

Since each fitted point is in the middle of the positive wave (that is the point on the surface of the pipeline), the range of the
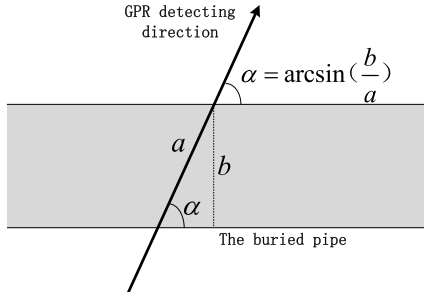
Fig. 11. Angle α between the pipe and the GPR's detecting direction could be calculated as $\arcsin\frac{b}{a}$, where a and b are the parameters of obtained ellipse equation as (3).

distance of each point could be set to be $\frac{d}{2}$, and the threshold of the sum of algebraic distance could then be calculated as $D_t = \frac{d}{2} \times n$, where n is the number of the points in $\mathbf{P}$.

D. Procedure of EIIA

Based on the abovementioned ellipse fitting algorithm and coordinate updating method, the procedure of the EIIA is presented in the following.

1) (Input) Point set $\mathbf{P} = \{P_i(x_i, y_i) | \ 0 \leq i \leq n\}$ extracted from the GPR B-scan image; the maximum number of iterations K; the threshold of the sum of algebraic distance D_t.
2) (Ellipse Fitting) Fit $\mathbf{P}$ into the ellipse by the proposed ellipse fitting algorithm, along which the sum of algebraic distance $D(\mathbf{P})$ from each point in $\mathbf{P}$ to the fitted ellipse is obtained.
3) (Coordinate Updating) Updating the coordinates of each point in $\mathbf{P}$ from the middle vertex to both the left and right sides.
4) (Check for convergence) If the iterative number reaches K, or $D(\mathbf{P}) \leq D_t$, output the ellipse equation with the smallest $D(\mathbf{P})$. Otherwise, return to Step 2.

The angle α between the pipeline's orientation and the GPR's detecting direction could be calculated as $\arcsin\frac{b}{a}$ as Fig. 11, where a and b are the parameters of the obtained ellipse as (3), and b indicates the radius of the pipeline.

As Fig. 12 shows, for an obtained α, there are two possible pipeline orientations as the red and blue lines. Therefore, when choosing the detecting direction of GPR, we choose the direction that is not perpendicular to the pipeline according to the existing pipeline map, such as $\frac{4}{9}\pi$ or $\frac{3}{8}\pi$. The obtained pipeline's orientation that has a smaller angle with the orientation on the existing pipeline map is adopted as the modified pipeline's orientation, as the blue line in Fig. 12.

IV. EXPERIMENTAL STUDY

To evaluate the effectiveness of the proposed model, experiments are conducted in real-world areas. After that, the experimental results are analyzed, and the effect of permittivity on the accuracy of the proposed method and the comparative work is also presented.
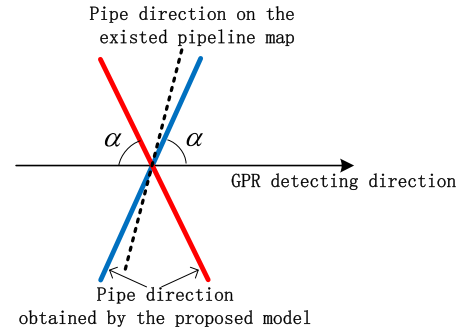

Fig. 12. Black line with an arrow indicates the direction of GPR, the blue and red lines represent two possible pipeline orientations, both of which have an angle of α with the GPR's detecting direction. The dashed line indicates the orientation of the pipeline on the pipeline map. The blue line is adopted as the pipeline's orientation, since it has smaller angle with the black dashed line compared with the red line.

Fig. 13. (a) and (b) Host, antenna, and odometer of the GSSI's SIR-30 GPR.

A. Experimental Settings on Real-World Datasets

The experiments are carried out on metal water supply pipelines, with the diameter between 60 cm to 100 cm. GSSI's SIR-30 GPR (see Fig. 13) is utilized to collect GPR B-scan images. In our experiments, the proposed model is combined with the GPR B-scan image interpreting method that has been detailed in our previous work [19]. Specifically, the permittivity is measured by detecting several underground pipelines in each area, selecting the image with clear hyperbolic characteristics, confirming their directions [28], then fitting the generated hyperbolic characteristics on the B-scan image. From the obtained GPR image, it could be observed that the underground medium of the selected are where the pipelines are located is basically uniform. The two selected areas with existing pipeline maps are shown in Fig. 14(a) and (b), where the detecting positions and directions are also presented.

B. Experimental Results and Analysis

When extracting point sets from the obtained GPR B-scan images, 30 points are extracted from the identified downward-opening signature. The maximum number K of iterations is set to 20, and the thresholds of the average ellipse fitting error are set to 3 to 8 cm. By applying the proposed model, the orientations of buried pipelines are obtained, by which the existing pipeline maps are modified. To validate the results, more detections are conducted as the red line with arrows in Fig. 14(a) and (b), and some evacuations are conducted to determine the actual orientation and radius of each pipeline. Due to the limitation of this article's length, the obtained GPR B-scan images could not

(a)

(b)

Fig. 14. (a) and (b) Two selected areas, existing and revised pipeline maps. The black lines indicate the pipelines on the existing pipeline map. The green lines with arrows indicate the GPR's detecting direction and position. The red dashed lines are the modified pipelines, and the red arrows indicate some more detections conducted to validate the obtained results.

(a)   (b)   (c)
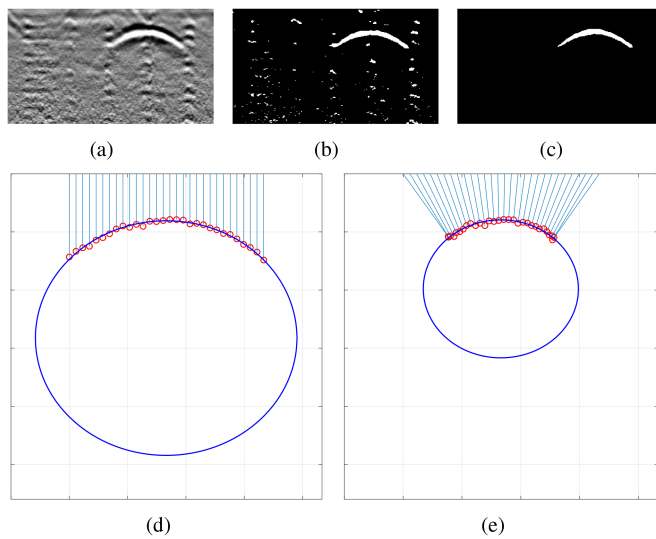
(d)   (e)

Fig. 15. Processing flow of the proposed model. (a) B-scan image. (b) and (c) Thresholded image and the obtained result after preprocessing, OSCA and PFJ. (d) Extracted point set and the fitted ellipse at the beginning of the iteration. (e) Result of the proposed model, where the extracted points are inverted to the elliptical cross-section of the pipe.

TABLE I
ERRORS OF THE PROPOSED MODEL

Area	The average error		The max error	
	Directions(α)	Radius(b)	Directions(α)	Radius(b)
1	4.03%	5.23%	7.14%	7.22%
2	5.10%	5.90%	8.40%	7.41%

be fully demonstrated here, and images that illustrate the process of the proposed model are shown in Fig. 15. In Figs. 16 and 17, two more examples are presented. The measured errors of the conducted experiments are presented in Table I.

In the conducted experiments, the error of orientations obtained by the proposed model could be controlled at about 5% in the experimental environments of this article. This is of practical value in real-world applications, since only one detection is needed to confirm the general orientation of the pipeline, and provides a basis for detection at the next position. If a hyperbolic
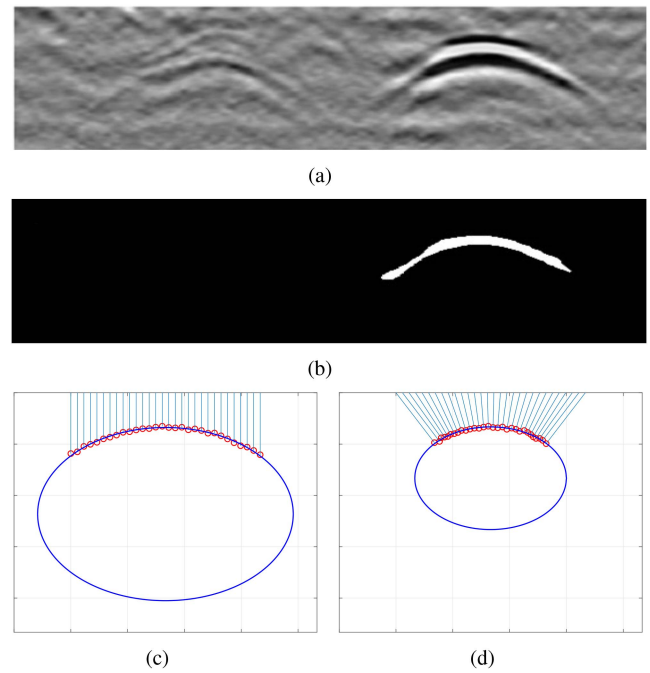

(a)

(b)

(c)   (d)

Fig. 16. (a) and (b) B-scan image and the obtained result after preprocessing, OSCA and PFJ. (c) Extracted point set and the fitted ellipse at the beginning of the iteration. (d) Result of the proposed model, where the extracted points are inverted to the elliptical cross-section of the pipe.

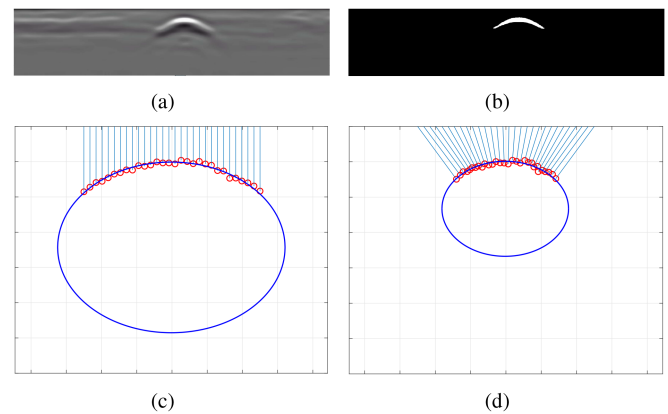(a)   (b)

(c)   (d)

Fig. 17. (a) and (b) are the B-scan image and the obtained result after preprocessing, OSCA, and PFJ. (c) is the extracted point set and the fitted ellipse at the beginning of the iteration. (d) is the result of the proposed model, where the extracted points are inverted to the elliptical cross-section of the pipe.

fitting method is used to confirm the radius and orientation of the pipeline, two measurements are required to determine the orientation, and one more measurement is needed to obtain the exact radius. In the conducted detections, all extracted point sets converge and launch iterations within 20 times. Moreover, when the permittivity of the soil is precisely known, the radius of the pipeline could be obtained through a detection that is not strictly required to be perpendicular to the pipeline's orientation.

In the process of iteration, the sum of the algebraic distances is generally decreased, that is, the accumulated error is also gradually reduced. The rate of decrease is fast first and then slow until the sum of the algebraic distances is stable. Fig. 18
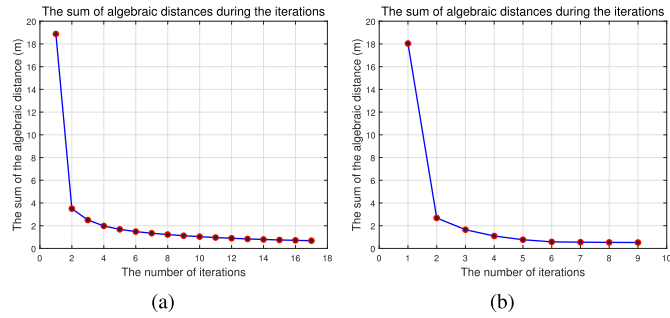
(a)   (b)

Fig. 18. (a) and (b) Two examples of the sum of algebraic distances during the iterations. It could be observed that the sum of the algebraic distances is generally decreased, that is, the accumulated error is also gradually reduced. The rate of decrease is fast at first (especially in the first iteration) and then slow until the sum of the algebraic distances is stable.

TABLE II
ERRORS OF THE PROPOSED MODEL AT DIFFERENT NOISES ON THE
SUBSURFACE PERMITTIVITY

Noise Level		5%	8%	10%	15%	20%
Average error (%)	Radius	6.12	6.92	8.11	22.14	33.12
	Directions	8.12	8.52	9.12	20.17	29.32
Max error (%)	Radius	7.11	8.15	10.21	29.15	39.12
	Directions	10.21	10.82	10.92	22.48	41.21

shows two examples of the sum of algebraic distances during the iterations.

The abovementioned experimental results are obtained based on the fact that the underground permittivity in the experimental area does not change significantly, that is, there is no obvious layering on the GPR B-scan image at the underground depth where the pipeline is located. In order to evaluate the effect of the proposed method under more complex noisy conditions. We added Gaussian noises with different levels to the subsurface permittivity and evaluate the effectiveness of the proposed method. The errors under different noise levels are presented in Table II.

When the error of the measured underground permittivity is less than 10%, the method proposed in this article can obtain reliable results (the maximum error is controlled at about 10%). However, when the error of the underground permittivity is greater than 15%, the error of the method proposed in this article is relatively large. These experimental results show that the applicable condition of the proposed method is limited to the experimental area where the underground permittivity does not change significantly, and accurate measurement of the underground permittivity is required. On the basis of the above, the method in this article is utilized, and the results could be reliable.

In practical applications, there is a situation that might occur, that is, the downward-opening point clusters is directly fitted to a hyperbola to estimate the pipeline (even if the detection direction of the GPR is not perpendicular to the pipeline direction). To evaluate the performance of our method in measuring the pipeline's radius compared with the hyperbolic fitting methods. The restricted algebraic-distance-based fitting algorithm (RADF) [19] and orthogonal-distance-based fitting (ODF)

TABLE III
AVERAGE ERROR OF RADIUS BY RADF, ODF, AND EIIA

| Area | The average error of radius | | |
	ODF	RADF	EIIA
1	15.20%	13.25%	**5.23%**
2	17.31%	15.59%	**5.90%**

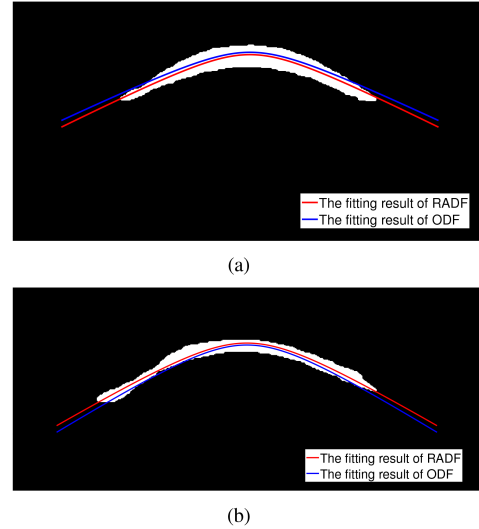Results with minimal errors are bolded.

(a)

(b)

Fig. 19. (a) and (b) Fitting results obtained by RADF and ODF on two obtained point clusters. It could be observed that the fitting results are quite similar. If the point cluster is regarded as a hyperbola, the hyperbolic fitting result is basically consistent with the point cluster.

method [10] are also applied to fit the extracted point sets to estimate the radius of the pipe, and the results are shown in Table III. Fig. 19 illustrates examples of the fitting results obtained by RADF and ODF.

It could be observed from Table III that when the GPR's detecting direction is not perpendicular to the pipeline, fitting the generated features by hyperbolic equations would leads to larger errors than the proposed model. However, as shown in Fig. 19, the results of the hyperbolic fitting by RADF and ODF are both basically consistent with the point cluster with downward opening, although the actual error could be obvious as presented in Table III. These fitting results would cause confusion in real-world applications. When the pipeline is not perpendicular to the detecting direction of GPR, although it is intuitively possible to use a hyperbola to fit the point set and match it, but through this, there will be errors in the calculated underground permittivity and the depth or radius of the pipeline. This error is mainly related to the angle of the GPR and the pipeline. In the case where the permittivity of the detection area has been measured, more accurate results could be achieved using the method proposed in this article.

V. CONCLUSION

In this article, a novel method to estimate the orientation and radius of the buried pipeline from GPR B-scan image is proposed. The proposed model could be carried out on the basis

of obtaining the subsurface permittivity of the detected area. The model consists of the following two parts: GPR B-scan image processing and EIIA. The GPR B-scan image is first processed with the downward-opening point set extracted. Then, the obtained point set is iteratively inverted to the cross-section of the buried pipe, that is, the elliptical cross-section caused by the angle between the GPR's detecting directions and the pipeline's orientations. By minimizing the sum of the algebraic distances from these points to the inverted ellipse, the most likely orientation and radius of the target pipeline are determined. Experiments on real-world datasets are conducted, and the existing pipeline maps are modified, which validated the effectiveness of the proposed model. Moreover, we also verified that the effect of using the proposed method could be affected by the accuracy of the obtained permittivity. Therefore, it is a necessary condition for the proposed method to accurately measure the underground permittivity of the detection area. In practical applications, the proposed method could be combined with the GPR B-scan image interpreting model that has been detailed in our previous work [19], that is, to measure a certain pipeline accurately to obtain the permittivity, and then use the method proposed in this article to detect other pipes in the detection area. In future work, we will focus on mapping pipelines of an area where there is no existing pipeline map.

REFERENCES

[1] F. Soldovieri, J. Dumoulin, N. Masini, and E. Utsi, "Noninvasive sensing techniques and geophysical methods for cultural heritage and civil infrastructures monitoring," *Int J. Geophys.*, vol. 2011, 2011, Art. no. 487679.

[2] T. Hao, W. Zheng, W. He, and K. Lin, "Air-ground impedance matching by depositing metasurfaces for enhanced GPR detection," *IEEE Trans. Geosci. Remote Sens.*, vol. 58, no. 6, pp. 4061–4075, Jun. 2020.

[3] S. Shihab and W. Al-Nuaimy, "Radius estimation for cylindrical objects detected by ground penetrating radar," *Subsurface Sens. Technol. Appl.*, vol. 6, no. 2, pp. 151–166, 2005.

[4] G. Borgioli, L. Capineri, P. Falorni, S. Matucci, and C. Windsor, "The detection of buried pipes from time-of-flight radar data," *IEEE Trans. Geosci. Remote Sens.*, vol. 46, no. 8, pp. 2254–2266, Aug. 2008.

[5] C. Windsor, L. Capineri, and P. Falorni, "A data pair-labeled generalized hough transform for radar location of buried objects," *IEEE Geosci. Remote Sens. Lett.*, vol. 11, no. 1, pp. 124–127, Jan. 2014.

[6] H. Youn and C. Chen, "Automatic GPR target detection and clutter reduction using neural network," in *Proc. 9th Int. Conf. Ground Penetrating Radar Int. Soc. Opt. Photon.*, 2002, pp. 579–582.

[7] E. Pasolli, F. Melgani, and M. Donelli, "Automatic analysis of GPR images: A pattern-recognition approach," *IEEE Trans. Geosci. Remote Sens.*, vol. 47, no. 7, pp. 2206–2217, Jul. 2009.

[8] C. Maas and J. Schmalzl, "Using pattern recognition to automatically localize reflection hyperbolas in data from ground penetrating radar," *Comput. Geosci.*, vol. 58, pp. 116–125, 2013.

[9] H. Chen and A. Cohn, "Probabilistic conic mixture model and its applications to mining spatial ground penetrating radar data," in *Proc. Workshops SIAM Conf. Data Mining*, 2010, pp. 1–9.

[10] Q. Dou, L. Wei, D. Magee, and A. Cohn, "Real time hyperbolae recognition and fitting in GPR data," *IEEE Trans. Geosci. Remote Sens.*, vol. 55, no. 1, pp. 51–62, Jan. 2017.

[11] X. Zhou, H. Chen, and T. Hao, "Efficient detection of buried plastic pipes by combining GPR and electric field methods," *IEEE Trans. Geosci. Remote Sens.*, vol. 57, no. 6, pp. 3967–3979, Jun. 2019.

[12] D. Daniels, "Ground penetrating radar," *Inst. Eng. Technol.*, vol. 1, pp. 1–13, 2004.

[13] C. Bruschini, B. Gros, F. Guerne, P. Pièce, and O. Carmona, "Ground penetrating radar and imaging metal detector for antipersonnel mine detection," *J. Appl. Geophys.*, vol. 40, no. 1, pp. 59–71, 1998.

[14] D. Ramaccia, C. Guattari, F. Bilotti, and A. Toscano, "A new tool for the retrieval of effective permittivity of ground by using a commercial GPR," in *Proc. IEEE Antennas Propag. Soc. Int. Symp.*, 2013, pp. 1148–1149.

[15] P. D. Walker and M. R. Bell, "Subsurface permittivity estimation from ground-penetrating radar measurements," in *Conf. Rec. IEEE Int. Radar Conf.*, 2000, pp. 341–346.

[16] T. W. Caffey, "A range algorithm for ground penetrating radar," in *Proc. Int. Geosci. Remote Sens. Symp.*, 1996, vol. 4, pp. 2023–2026.

[17] A. Tzanis et al., "MATGPR: A freeware MATLAB package for the analysis of common-offset GPR data," *Geophys. Res. Abstr.*, vol. 8, 2006, Art. no. 09448.

[18] H. Chen and A. Cohn, "Probabilistic robust hyperbola mixture model for interpreting ground penetrating radar data," in *Proc. Int. Joint Conf. Neural Netw.*, 2010, pp. 1–8.

[19] X. Zhou, H. Chen, and J. Li, "An automatic GPR B-scan image interpreting model," *IEEE Trans. Geosci. Remote Sens.*, vol. 56, no. 6, pp. 3398–3412, Jun. 2018.

[20] H. Chen and A. G. Cohn, "Buried utility pipeline mapping based on multiple spatial data sources: A Bayesian data fusion approach," in *Proc. Int. Joint Conf. Artif. Intell.*, 2011, vol. 11, pp. 2411–2417.

[21] Q. Dou et al., "3D buried utility location using a marching-cross-section algorithm for multi-sensor data fusion," *Sensors*, vol. 16, no. 11, 2016, Art. no. 1827.

[22] X. Zhou, H. Chen, and J. Li, "Probabilistic mixture model for mapping the underground pipes," *ACM Trans. Knowl. Discov. Data*, vol. 13, no. 5, pp. 1–26, 2019.

[23] X. Zhou, Q. Chen, S. Lyu, and H. Chen, "Mapping the buried cable by ground penetrating radar and Gaussian-process regression," *IEEE Trans. Geosci. Remote Sens.*, vol. 60, 2022, Art. no. 4509912.

[24] Y. Yu, C.-C. Chen, X. Feng, and C. Liu, "Application of entropy classification method to the detection of subsurface linnear targets in polarimetric GPR data," in *Proc. IEEE Int. Geosci. Remote Sens. Symp.*, 2016, pp. 7438–7441.

[25] P. Farinelli and F. Roth, "Frequency domain analysis of the polarimetric ground-penetrating radar response of landmines and minelike targets," in *Detection and Remediation Technologies for Mines and Minelike Targets VIII*, vol. 5089, Bellingham, WA, USA, 2003, pp. 437–447.

[26] S. J. Seol, J.-H. Kim, Y. Song, and S.-H. Chung, "Finding the strike direction of fractures using GPR," *Geophys. Prospecting*, vol. 49, no. 3, pp. 300–308, 2001.

[27] H. Liu, X. Huang, F. Han, J. Cui, B. F. Spencer, and X. Xie, "Hybrid polarimetric GPR calibration and elongated object orientation estimation," *IEEE J. Sel. Topics Appl. Earth Observ. Remote Sens.*, vol. 12, no. 7, pp. 2080–2087, Jul. 2019.

[28] H. Chen and A. G. Cohn, "Buried utility pipeline mapping based on street survey and ground penetrating radar," in *Proc. 19th Eur. Conf. Artif. Intell. Front. Appl.*, 2010, vol. 215, pp. 987–988.

[29] G. Olhoeft, "Maximizing the information return from ground penetrating radar," *J. Appl. Geophys.*, vol. 43, no. 2, pp. 175–187, 2000.

[30] A. Strange, V. Chandran, and J. Ralston, "Signal processing to improve target detection using ground penetrating radar," in *Proc. 4th Australas. Workshop Signal Process. Appl.*, 2002, pp. 139–143.

[31] R. Gonzalez and R. Woods, "Image processing," in *Digital Image Processing*, vol. 2, New York, USA: Pearson Education, 2007.

[32] W. Gander, G. Golub, and R. Strebel, "Least-squares fitting of circles and ellipses," *BIT Numer. Math.*, vol. 34, no. 4, pp. 558–578, 1994.

[33] M. Grant and S. Boyd, "Graph implementations for nonsmooth convex programs," in *Recent Advances in Learning and Control*. Berlin, Germany: Springer, 2008, pp. 95–110.

[34] A. Y. Uteshev and M. V. Goncharova, "Point-to-ellipse and point-to-ellipsoid distance equation analysis," *J. Comput. Appl. Math.*, vol. 328, pp. 232–251, 2018.

Xiren Zhou received the B.Sc. degree from Shandong University, Jinan, China, in 2014 and the Ph.D. degree in computer science from the University of Science and Technology of China (USTC), Hefei, China, in 2019.

He is currently an Associate Researcher with the School of Computer Science and Technology, USTC. His research interests include machine learning, ground-penetrating radar, and multisensor data fusion.

Qiuju Chen received the B.Sc. degree from the School of Information Science and Technology, University of Science and Technology of China, Hefei, China and the Ph.D. degree from the National University of Defense Technology, Changsha, China, in 2004 and 2016, respectively, both in signal and information processing.

She is currently an Associate Research Fellow with the University of Science and Technology of China. Her research interests include relation extraction and machine learning.

Shengfei Lyu received the B.Sc. degree in information management and information systems from the Hefei University of Technology, Hefei, China, in 2015 and the Ph.D. degree in computer science from the School of Computer Science and Technology, University of Science and Technology of China, Hefei, in 2020.

He is currently a Research Fellow of Nanyang Technological University (NTU), Singapore. His research interests include relation extraction, data mining, and machine learning.

Huanhuan Chen (Senior Member, IEEE) received the B.Sc. degree in electronic engineering and information science from the University of Science and Technology of China (USTC), Hefei, China, in 2004 and the Ph.D. degree in computer science from the University of Birmingham, Birmingham, U.K., in 2008.

He is currently a Full Professor with the School of Computer Science and Technology, USTC. His current research interests include neural networks, Bayesian inference, and evolutionary computation.

Dr. Chen was the recipient of the 2015 International Neural Network Society Young Investigator Award, the 2012 IEEE Computational Intelligence Society Outstanding Ph.D. Dissertation Award, IEEE TRANSACTIONS ON NEURAL NETWORKS Outstanding Paper Award (bestowed in 2011 and only one paper in 2009), and the 2009 British Computer Society Distinguished Dissertations Award. He is currently an Associate Editor for IEEE TRANSACTIONS ON NEURAL NETWORKS AND LEARNING SYSTEM, and IEEE TRANSACTIONS ON EMERGING TOPICS IN COMPUTATIONAL INTELLIGENCE.